

Smart Branching

An Experimental Method for Heterogeneous Branching Networks using Non-planar 3D Printed Clay Deposition

Chenxiao Li
University of Pennsylvania

Mingyang Yuan
University of Pennsylvania

Zilong Han
University of Pennsylvania

Billie Faircloth
KieranTimberlake
& University of Pennsylvania

Jeffrey S. Anderson
University of Pennsylvania
& Pratt Institute

Nathan King
University of Pennsylvania
& Virginia Tech

Robert Stuart-Smith
University of Pennsylvania
& University College London

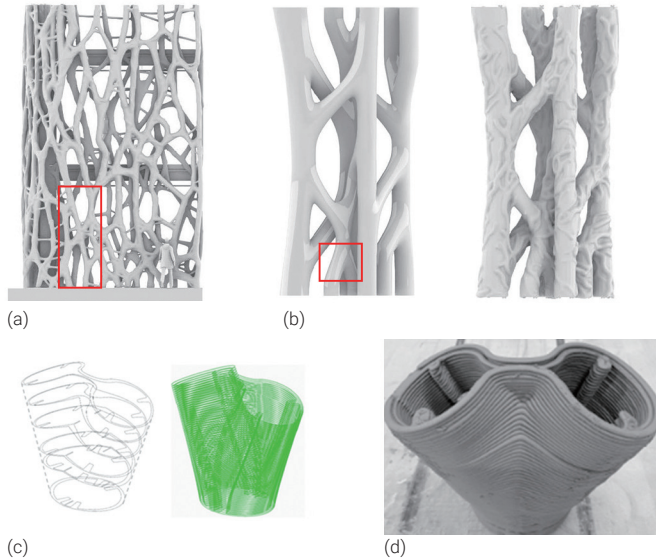


ABSTRACT

Clay extrusion 3D printing with 6-axis industrial robots and ceramic firing pipelines has inspired designers' reflection on material properties, design methodologies, automatic manufacturing, and logistics of fabrication. It brings the potential for innovative industrial bespoke production of architectural components. Plasticity and malleability are merits to the creative freedom of the form, yet they also pose technical challenges. The goals of the research are designing specifically printable geometries at a durable scale and optimizing methodologies for fabrication to ensure both quality and efficiency.

Through the design and fabrication of a 1.3m-high physical prototype sampled from our facade proposal, we developed a relatively automated project pipeline. It aims to achieve the generative and evolutionary design and a non-planar clay deposition method for tubular branching components.

1 Photograph collection of 36 physical models produced using non-planar 3D printed clay deposition



2 Fabricating branching structures using clay extrusion 3D printing presents technical challenges at bifurcations: (a) Digital model of full scale architectural envelope proposal based on a customized method; (b) Digital model of the 1.3 m high prototype; (c) Double-layer print path for a 45° bifurcated branch component; and (d) Outcome of 45° bifurcated branch component produced using non-planar 3d printed deposition

INTRODUCTION

Branch-like geometries provide diverse structural, functional, and aesthetic potential for trussed, diagrid, or funicular structures. Clay extrusion 3D printing allows for variable manufacturing and can support heterogeneous arrangements of branch-like geometries (Bechthold 2016); however, several technical challenges exist in the fabrication of these geometries with clay extrusion 3D printing due to clay's plasticity and drying time.

Background and State of the Art

3D printed concrete and clay have similar types of plasticity when extruded; therefore, it is helpful to review advances in concrete 3D extrusion printing. 3D printing methods for concrete and ceramics both involve continuous extrusion. 3D printed concrete, often referred to as Chemical Reaction Bonding Concrete (CRB/C) and ceramic Liquid Deposition Modeling (LDM) both involve the use of an industrial extrusion screw and a liquid material reservoir that feeds the extruder. While concrete incorporates a mixer, clay LDM utilizes a cylindrical tank located on the robot adjacent to the extruder. Both can be performed on an industrial robotic arm to print on a flat floor, where the extrusion can be switched on or off by a digital signal (Kontovourkis and Tryfonos 2018). With a 6-axis industrial robotic arm, printing has fewer limitations: each extrusion layer is not necessarily limited to horizontal deposition. Therefore, it is possible to print ceramics and concrete on complex surfaces such as freeform foam shaped by a hotwire cutter on a robotic arm (Ko et al. 2018).

Research on the non-planar deposition of 3D printed concrete is far ahead of similar research in clay. In some projects, the more complex printing method of rotating the tool center point (TCP) plane is applied to bifurcated cylinders using sidestepping (Cruz et al. 2022). Helpful techniques have been developed in the past five years including changing the toolpath to optimize the surface (Zhong et al. 2020; Nisja et al. 2021) and exploring the printing of smaller bifurcated parts using planar 3D ceramics extrusion printing (Xing et al. 2021). Apart from non-planar 3D printing, printing on a movable build plate is also a notable FDM method (Nayyeri et al. 2022). However, remaining limitations are managing the plasticity and semi-liquid properties of clay to maintain balance during the printing process; the allowable inclination angle of geometries to avoid collapse; the need to prevent slumping of inclined parts due to gravity; and increasing the surface quality of the prints.

Experimental Overview

Our experiments prioritize the following questions:

- What are the precautions to prevent excessive deposition of clay during the printing to ensure the surface quality of each print?
- How can parts be balanced during the printing process? Through an automatically updated feedback loop with real sense scanning, is it possible to update the tool path according to design intent?
- What aspects of this fabrication pipeline could contribute to future industrial bespoke production?

Firstly, we conducted experiments to quantify the printing parameters, including changing TCP plane angles. Secondly, we utilized a sloped bed and differentiated the deposition thickness of the clay. We also used depth tracking (Intel RealSense™ depth camera D435) to detect deformations in inclined prints and adjust the printing path as needed. Finally, we completed the design and robotic fabrication of a prototype branching structure, incorporating findings from former experiments on the branching shape. The 1.3 m tall prototype is comprised of 37 components that demonstrate our approach to non-planar 3D clay extrusion printing (Figure 2).

MATERIALS AND METHODS

Clay Body and Firing Process

All tests are based on MC10G earthenware clay, and the shrinkage rate of 4.5% and a water absorption of $\pm 1\%$. The ratio we used for the mixture is 25 lbs clay to 16 oz water. They are inserted in a pug mill, Peter Pegger VPM-60 Power Wedger, for mixing with water for at least 2 hours. It is also worth noting that, from our tests, it is better to let the clay sit for more than 2 hours after being pugged out of the mill. The whole prototype can take up to 3 days for printing, and the printing time for each component is approximately 5-15 minutes. Each

component took 12-24 hours to be fully bone-dried depending on the amount of clay accumulated. After being bone dried, components are fired under cone 04 with temperature 1945 °F and then cooled down. The whole process of firing and cooling takes 24-36 hours.

Robotic Clay Extrusion

All robotic clay extrusion was done using 6-axis ABB IRB4600 industrial robot (ABB robot), with LDM WASP Extruder XL (WASP extruder) and a 5 liter Clay Tank (Figure 3). The cooperation with robots is through RobotStudio Online and FlexPendant.

Early Experiments

We conducted a series of tests on 3D printing parameters specific to ABB robot and WASP extruder, and observed that nozzle diameter (ND) of 4 mm, moving speed (MS) of 80%, layer height (LH) of 5.5 mm, and extruding speed (ES) of 9 worked best in all results for vertical cylinders of 10 cm diameter.

Subsequently, we conducted two experiments to test the limits of non-planar 3D deposition of a bifurcated tubular geometry: the first one testing the limitation of height, and the second testing the slope as the printing bed, as well as the branching angle of the bifurcation.

Experiments of Printing Cylinders

We printed cylinders of different heights with the same diameter and printing parameters, and concluded that the maximum viable height of printing a basic cylinder without any collapse is around 18 - 20 cm (Table 1).

Experiments of Printing Bifurcation on Slope

We printed cylinders and bifurcated tubes of 30°, 45°, and 60°

TABLE 1 Experiments on Scale Limitation

Test Number	Invariants	Height (center-meter)	Result	Detail
1		10	✓	no obvious deformation
2	NZ = 4mm, MS = 80%, LH = 5.5mm, ES = 9	15	✓	bottom is about 5% thicker
3		17.5	✓	bottom is about 15% thicker
4		20	×	unacceptable collapsing

on horizontal surfaces and slopes (Figure 4). To exclude interference of other uncertainties, such as different humidity of the clay body, we tested each print twice, and the result was recorded as a “✓” only if both prints were successful. Thus we found out that the relationship between angle and the slope is that the best choice for 30°, 45°, 60° bifurcation is a 10° slope.

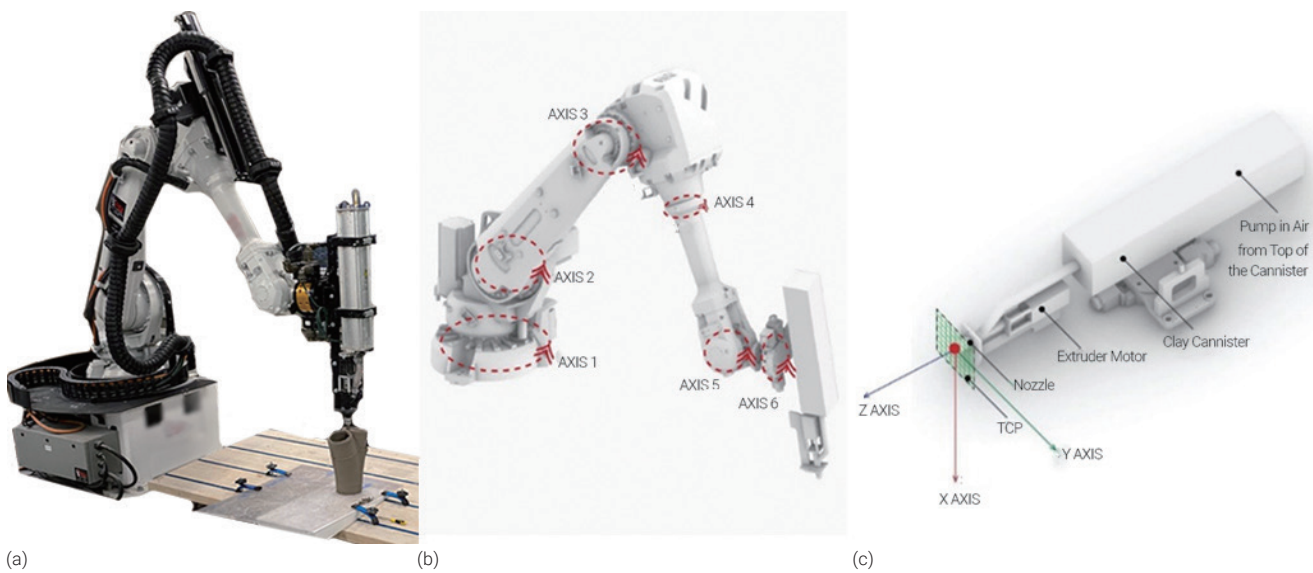
FINAL PROTOTYPE

Design to Fabrication Methodology

We describe a multi-step design to fabrication workflow that incorporates: 1) The generation of the branching pattern using cellular automata (CA), solar radiation analysis, and a self-organization algorithm; 2) The modelling of components uses SubD Multipipe in Rhinoceros 3D and an evolutionary algorithm to generate a structural augmented lattice network on top of the geometry; 3) A toolpath using non-planar slicing methods; 4) A bespoke 3D printing process using non-planar 3D printing with a sloped bed.

Branching Pattern Generation

To generate the branching pattern, we created a custom combination of cellular automata CA rules (Figure 5) based on Stephen



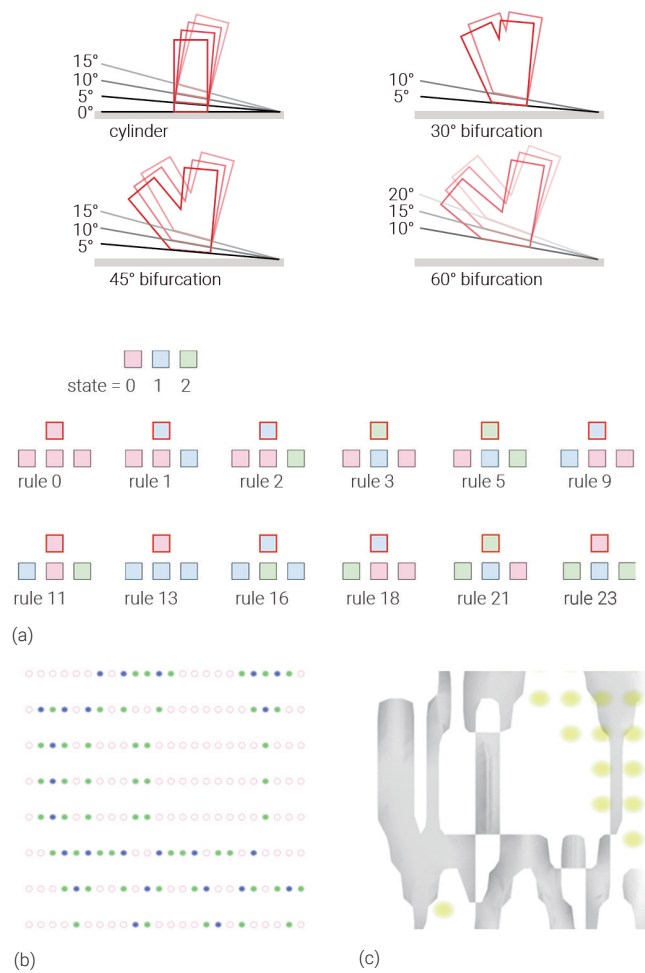
3 Robotics elements of the experiments: (a) 6-axis ABB IRB4600 industrial robot, (b) Digital model of 6-axis ABB IRB4600 noting each axis of rotation with clay extruder, (c) Details of the clay extruder with motor, nozzle, and canister.

Wolfram's 1D CAs with three possible CA cell states (0, 1 or 2) (Wolfram 2002) within a two-dimensional array of cells to produce a branching organization of cells of the same state. This first branching pattern was used to generate center-curves of the proposed networked branching ceramic assemblage.

To generate site specific bespoke design that respond to the related climate condition, we performed a solar radiation analysis with Ladybug Tools 1.4.0 (Ladybug Tools LLC 2022) on the branching pattern using the values to either attract or repel branches. The final branching pattern was used to generate center-curves of the proposed networked branching ceramic assemblage (Figure 6).

Modeling the Branching Prototype Components

All components were printed with a double-wall thickness:

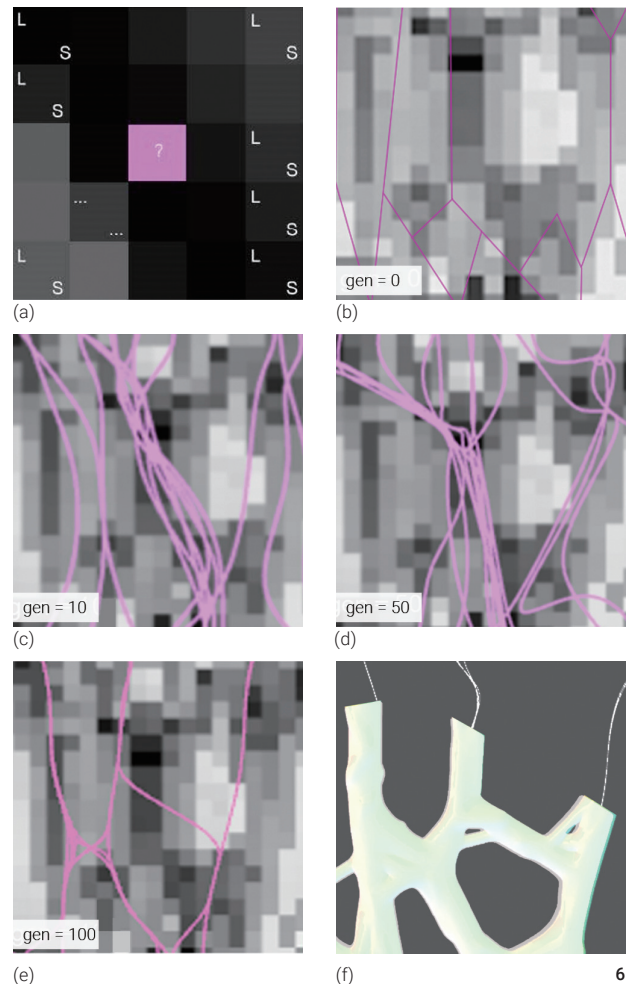


- Basic bifurcations were printed on different slopes of 0°, 5°, 10°, 15°, and 20°. Only succeeded experiments were listed in this diagram, and we can see that, firstly, slope can help balance the print; secondly, each slope of same degree has certain tolerance of branching degree of the prints.
- Generation of the branching pattern: (a) Each CA cell has three possible states (0, 1 or 2), and adjusts its own state based on the states of neighboring cells; (b) This two-dimensional array of cells can produce a branching organization of cells of the same state; and (c) Branching pattern from cells: the state 0 cell acts as a void, state 1 influencing a displacement of 5 cm, and state 2 influencing displacement of 10 cm

one 8 cm diameter tube for structural reinforcement, while the outer 10 cm diameter tube also embodied a variable ornamental pattern (Figure 2). The prototype is composed of 37 components that range from 5 cm to 30 cm tall, generated by splitting the interconnected branches based on two rules (Figure 10). Overall, "X" splits were horizontal and "Y" splits were vertical, and some components were generated by using both rules (Figure 9).

Generating Component Tool Paths

For branches whose centerline symmetry axis deviates from the absolute vertical line by an angle greater than 15° and whose height is greater than 10 cm, the digital model is first rotated by 10° and then the tool path is generated; if the height



- Generation of branching pattern: (a) Firstly, translate solar radiation analysis results into hue, saturation, lightness (HSL) images, so that the CA point can find the closest point on mesh (HSL image) and inherit its L-value, and then the CA points will attract or repel the control points on original curves (pink square); (b) Original curves based on the first branching pattern; (c)(d)(e) Iterations of self-organization with attractors from solar radiation analysis; and (f) Use the curves produced as center-curves of the basic pipes

is greater than 15cm, additional reinforcement structures need to be added internally for support. If the height is greater than 15cm, it is necessary to add an additional reinforcement structure for support inside. All others can generate toolpath routinely (Figure 9).

Printing Process

For truncated cylinders, non-planar 3D printing was implemented (Figure 10); bifurcated tubes were printed on a 10° slope with non-planar 3D printing (Figure 11). For truncated cylinders that are taller than 15 cm, a real-sense camera was used to 3D scan already printed layers so that the print-path could be automatically adjusted after finishing every 10 layers to ensure the desired geometry for each component could be successfully fabricated irrespective of individual layer settlement (Figure 12).

For assembly of the prototype, we adopted a post-tension system (Figure 13). For the connection, we use laser-cut acrylic sheets and 3D printed spherical nuts (Figure 14). The spherical nuts can rotate to embed in the acrylic holes (Figure 7).

RESULTS




We printed more than 40 components for the final prototype. Some parts failed due to deformations caused by incorrect storage or due to accidental breakage. Finally we printed 37 piece of clay extruded components within three days of duration (Figure 1)

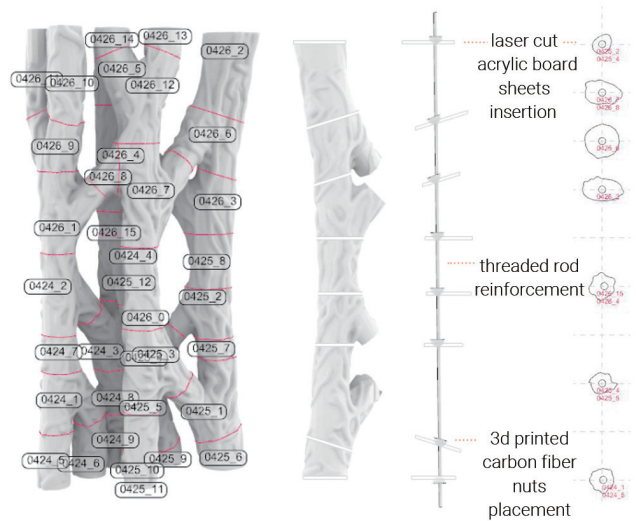
Clay Extrusion 3D Printing Parameter

For truncated and bifurcated branches, we found general printing parameters that allowed for successful production of components: nozzle diameter (ND) = 4 mm, moving speed (MS) = 80%, layer height (LH) = 5.5 mm, extruding speed (ES) = 9 (see Table 2). The most important note is that if $LH = 70\% - 90\% * ND$, the clay deposition performed best. For the toolpath design, we found that cracks easily appear at the corners of our tests. The comparison results show that a more rounded curve/chamfer tool path can avoid cracking at sharp corners (fillet radius > nozzle diameter).

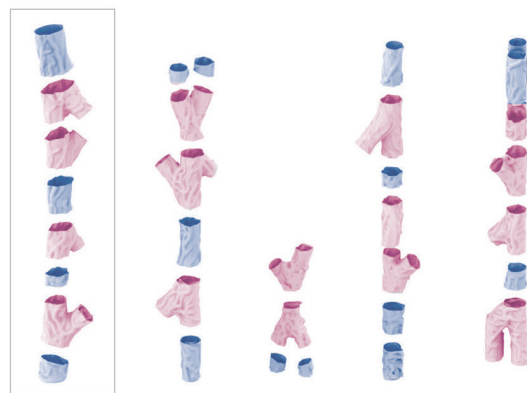
For the printing bed tests, we found that for our bespoke bifurcation—one vertical branch, another one bent (Figure 16)—when we ignore the potential uneven deposition or slight deformation in the printing process, the 10° slope works for

TABLE 2 Experiments on printing variables

Test Number	Invariants	Value	Detail
1-1	Layer Height	[2.0mm, 3.5mm, 5.0mm]	
1-2	Extruding Speed	[3, 6, 9]	
1-3	Moving Speed	[30%, 60%, 90%]	



7



8

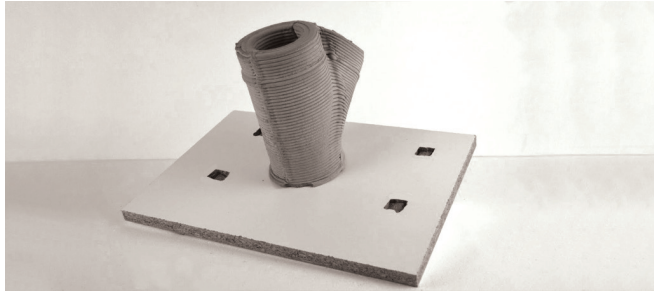


9

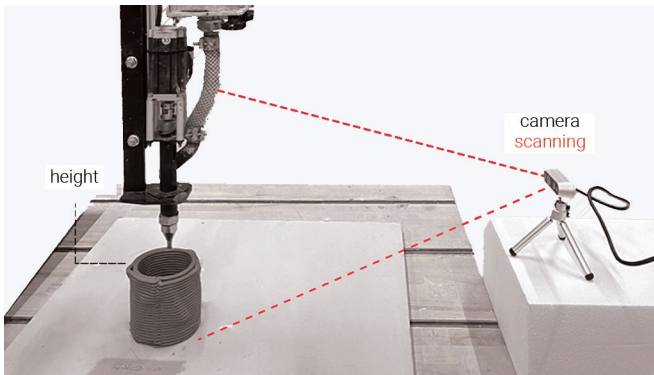
- (left) The slicing follows two rules: split branches horizontally if they incorporate a post-tensioning rod, if not, then split branches perpendicular to their normal; (right) Example of one column: Post-tensioned system inside one vertical branch and customized partitions, sphere nuts and acrylic sheets, for these components
- By following the slicing rules, all sliced segments for printing only have two different basic shapes: "I" (cylinder or truncated cylinder) or "Y" (bifurcated cylinder)
- The generation routine of non-planar print-path for "Y"



10



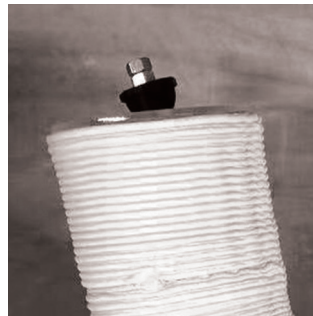
11



12



13



14

10 Non-planar 3D print deposition Method 1: Non-planar 3D print

11 Non-planar 3D print deposition Method 2: Printing on slope

12 Non-planar 3D print deposition Method 3: Using Intel RealSense RGBD camera to recalibration

13 Assembly of clay segments: First, we used customized sphere nuts to fix the four post-tensioned rods on the base, and then place each layer of clay segments, acrylic sheets and nuts from bottom to top

14 Physical partitions samples using 1/8 inch acrylic sheets and 3D printed 1 inch diameter and 1/2 inch thick spherical nuts

all branching prints (Table 3). It significantly improves the balance in the printing process (Figure 11).

Workflow

The non-planar deposition methods have been beneficial in our bespoke process. Firstly, non-planar printing effectively avoids over-squeezing and collapsing and improves the performance of truncated and bifurcated segments (Figure 16). Also, a continuous non-planar print path ensured the high efficiency of production. The addition of the slope helped some bifurcations that were difficult to balance to be produced successfully (Figure 2).

However, some identified issues necessitate further research. The real-sense camera used for recalibration was not accurate enough. It proved difficult to check the scan height in the camera's real-time feedback image during continuous clay extrusion. Therefore, we tried to introduce a pause in printing after each 10 completed layers to conduct a periodic scan and update the height of the robot's tool path for subsequent layers. The algorithm at this stage is not fully automated, with many parameters still requiring manual inputs.

CONCLUSION

In the three non-planar deposition methods we used for our bifurcated tubes, non-planar printing has been successfully achieved without substantial collapse or material settlement (Figure 15); however, further experiments should be carried out to ascertain a universal solution for more complex branching forms.

In the printing-on-slope method, the slope setting clearly brings a better balance and improves the success rate. However, there are also problems of complex calibration, increased resources, and wasted time. The initial position of the print is prone to errors, and even a few millimeters of error can result in insufficient adhesion or over-squeezing of the initial layers, thus affecting the stability and quality of subsequent prints. Following every printed component on a slope, one needs to wait for the clay body to dry out before transferring it to the flat floor. Therefore, we needed to prepare a lot of additional slopes.

Due to the low-resolution real-sense camera, we have only conducted the digital part of the experiment so far. The actual simulation requires a very clean background, and the presence of stray colors can lead to significant scanning errors, which left us with a question. If this technical problem can be solved, we can further combine non-planar printing, printing on the slope, and real-time recalibration to create a truly autonomous non-planar deposition printing system. This helps enrich the morphological diversity of ceramic branching structures, increasing the applicability of clay extrusion 3D printing.



- 15 Comparison between different approaches to non-planar 3D printing shows that we are able to control non-planar 3D printing for the desired results through updates in TCP and toolpath
- 16 Two representative comparison of before and after adopting our methods of improving the printing equality: (a) 1-1 test slumping result; (b) 1-3 test result, successfully maintaining the balance; (c) Horizontal 3D printing; and (d) non-planar printing results without over-squeezing

15

TABLE 3 Experiments on different degrees of branching and printing beds.

Test Number	Degree of Slope	Degree of Branching	Result	Observation
1-1	0°	30°	×	slumped at very last moment
1-2	5°	30°	✓	no slumping observed
1-3	10°	30°	✓	no slumping observed
1-4	15°	30°	×	collapsed from the bending side
1-5	20°	30°	×	collapsed from the bending side
2-1	0°	45°	×	slumped at 60% printing
2-2	5°	45°	✓	no slumping observed
2-3	10°	45°	✓	no slumping observed
2-4	15°	45°	✓	sinking at bending branch slightly
2-5	20°	45°	×	collapsed from the bending side
3-1	0°	60°	×	slumped
3-2	5°	60°	×	slumped
3-3	10°	60°	✓	sinking at bending branch slightly
3-4	15°	60°	✓	no slumping observed
3-5	20°	60°	✓	no slumping observed

ACKNOWLEDGMENTS

This research was undertaken in the Masters of Science in Design: Robotics and Autonomous Systems (MSD-RAS) program, at the University of Pennsylvania. Authors Li, Yuan, and Han were students in the program. Faircloth, Anderson, King, and Stuart-Smith were instructors who contributed to the research project and paper during and post studies. The authors also wish to thank teaching assistant David Forero and former student Yuxuan Wang for their support and input into the research.

REFERENCES

Bechthold, Martin, Anthony Kane, and Nathan King. 2015. *Ceramic Material Systems in Architecture and Interior Design*. Basel: Birkhauser.

Cruz, Paulo J. S., Bruno Figueiredo, João Moreira, and Samuel Ribeiro. 2022. "Ficus Columns." Accessed June 1, 2022. <https://www.aclab-idegui.org/ficus-columns>.

Ko, Minjae, Donghan Shin, Hyunguk Ahn, and Hyungwoo Park. 2018. "InFormed Ceramics: Multi-Axis Clay 3D Printing on Freeform Molds."

In *Robotic Fabrication in Architecture, Art and Design 2018*, edited by J. Willman, P. Block, M. Hutter, K. Byrne, and T. Schork. Cham: Springer Nature. 297–308.

Kontourourkis, Odysseas, and George Tryfonos. 2018. "Integrating Parametric Design with Robotic Additive Manufacturing for 3D Clay Printing: An Experimental Study." In *2018 Proceedings of the 35th International Symposium on Automation and Robotics in Construction (ISARC)*. Berlin, Germany. 918–925.

Ladybug Tools LLC. 2022. Ladybug Tools V. 1.4.0. <http://www.ladybug-tools/>.

Nayyeri, Pooyan, Kouros Zareinia, and Habiba Bougherara. 2022. "Planar and Nonplanar Slicing Algorithms for Fused Deposition Modeling Technology: A Critical Review." *The International Journal of Advanced Manufacturing Technology* 119 (5–6): 2785–2810.

Nisja, Georg Aarnes, Anni Cao, and Chao Gao. 2021. "Short Review of Nonplanar Fused Deposition Modeling Printing." *Material Design & Processing Communications* 3 (4): e221.

Wolfram, Stephen. 2002. *A New Kind of Science*. Champaign, IL: Wolfram Media.

Xing, Yu, Yu Zhou, Xin Yan, Haisen Zhao, Wenqiang Liu, Jingbo Jiang, and Lin Lu. 2021. "Shell Thickening for Extrusion-Based Ceramics Printing." *Computers & Graphics* 97: 160–69. <https://doi.org/10.1016/j.cag.2021.04.031>.

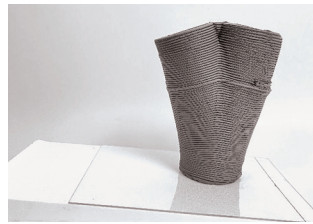
Zhong, Fanchao, Wenqiang Liu, Yu Zhou, Xin Yan, Yi Wan, and Lin Lu. 2020. "Ceramic 3D Printed Sweeping Surfaces." *Computers & Graphics* 90: 108–15. <https://doi.org/10.1016/j.cag.2020.05.007>.

IMAGE CREDITS

All drawings and images by the authors.



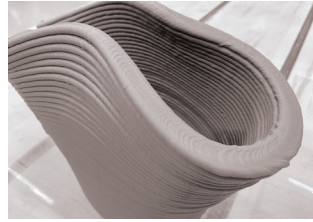
(a)



(b)



(c)



(d)

16

Chenxiao Li is a recent graduate of Master of Science in Design: Robotics and Autonomous Systems program from University of Pennsylvania. She is a Research Assistant focusing on computational design and robotics fabrication.

Mingyang Yuan is a Research Assistant in the Autonomous Manufacturing Lab at the University of Pennsylvania. She graduated with a Master of Architecture, and continued studying at the Master of Science in Design: Robotics and Autonomous Systems program.

Zilong Han is an architecture graduate student from University of Pennsylvania who believes technology will change the world.

Billie Faircloth is a practicing architect, and partner at KieranTimberlake, where she leads transdisciplinary research, design, and problem-solving processes across fields, including environmental management, chemical physics, materials science, and architecture. She is also a Adjunct Professor at University of Pennsylvania Weitzman School of Design.

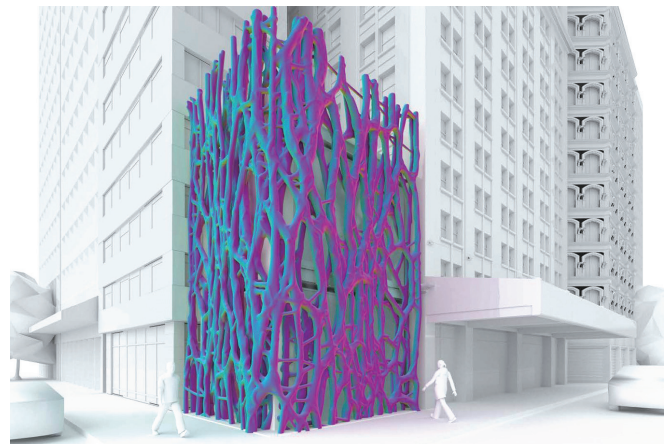
Jeffrey S. Anderson currently teaches design studios and advanced media seminars in the Graduate Architecture and Urban Design program at Pratt Institute and the Graduate Architecture Program at the University of Pennsylvania.

Nathan King is the Co-Director of the Center for Design Research at Virginia Tech, an Instructor at the University of Pennsylvania and Harvard University, and leads the Autodesk Research organization focusing on the Industrialization of Construction.

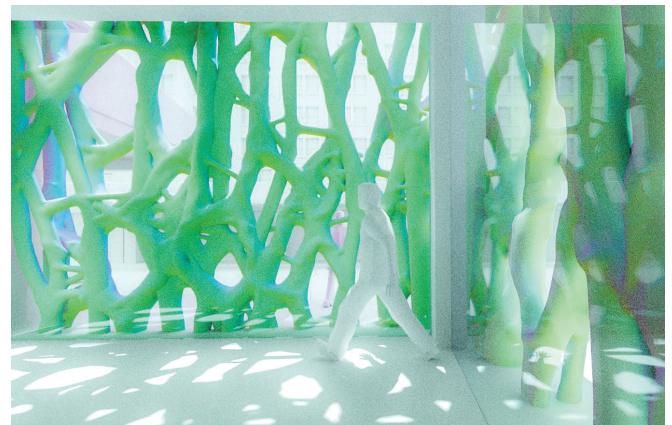
Robert Stuart-Smith is Director of the MSD-RAS program at the University of Pennsylvania, Director of the Autonomous Manufacturing Lab (AML) at Penn (Architecture), and Co-Director of the AML at University College London (Computer Science).



17



18



19

17 Final 1.3 m high ceramic assembly prototype

18 Facade proposal: exterior

19 Facade proposal: interior